Fluorescence Resonance Energy Transfer between Residues on Troponin and Tropomyosin in the Reconstituted Thin Filament: Modeling the Troponin–Tropomyosin Complex

ARTICLE *in* JOURNAL OF MOLECULAR BIOLOGY · MARCH 2008

Impact Factor: 4.33 · DOI: 10.1016/j.jmb.2007.10.078 · Source: PubMed

doi:10.1016/j.jmb.2007.10.078 J. Mol. Biol. (2008) 376, 80–91

JMB

Available online at www.sciencedirect.com

ScienceDirect

ELSEVIER

Fluorescence Resonance Energy Transfer between Residues on Troponin and Tropomyosin in the Reconstituted Thin Filament: Modeling the Troponin–Tropomyosin Complex

Chieko Kimura-Sakiyama[1]†, Yutaka Ueno[2]†, Katsuzo Wakabayashi[3] and Masao Miki[1,4]*

[1]*Division of Applied Chemistry and Biotechnology, Graduate School of Engineering Science, Fukui University, Fukui 910-8507, Japan*

[2]*Neuroscience Research Institute, National Institute of Advanced Industrial Science and Technology, Tsukuba 305-8568, Japan*

[3]*Division of Biophysical Engineering, Graduate School of Engineering Science, Osaka University, Toyonaka, Osaka 560-8531, Japan*

[4]*Research and Education Program for Life Science, Fukui University, Fukui 910-8507, Japan*

Received 3 September 2007; received in revised form 24 October 2007; accepted 28 October 2007
Available online 4 November 2007

Edited by M. Moody

Troponin (Tn), in association with tropomyosin (Tm), plays a central role in the calcium regulation of striated muscle contraction. Fluorescence resonance energy transfer (FRET) between probes attached to the Tn subunits (TnC, TnI, TnT) and to Tm was measured to study the spatial relationship between Tn and Tm on the thin filament. We generated single-cysteine mutants of rabbit skeletal muscle α-Tm, TnI and the β-TnT 25-kDa fragment. The energy donor was attached to a single-cysteine residue at position 60, 73, 127, 159, 200 or 250 on TnT, at 98 on TnC and at 1, 9, 133 or 181 on TnI, while the energy acceptor was located at 13, 146, 160, 174, 190, 209, 230, 271 or 279 on Tm. FRET analysis showed a distinct Ca^{2+}-induced conformational change of the Tm–Tn complex and revealed that TnT60 and TnT73 were closer to Tm13 than Tm279, indicating that the elongated N-terminal region of TnT extends beyond the beginning of the next Tm molecule on the actin filament. Using the atomic coordinates of the crystal structures of Tm and the Tn core domain, we searched for the disposition and orientation of these structures by minimizing the deviations of the calculated FRET efficiencies from the observed FRET efficiencies in order to construct atomic models of the Tn–Tm complex with and without bound Ca^{2+}. In the best-fit models, the Tn core domain is located on residues 160–200 of Tm, with the arrowhead-shaped I-T arm tilting toward the C-terminus of Tm. The angle between the Tm axis and the long axis of TnC is ~75° and ~85° with and without bound Ca^{2+}, respectively. The models indicate that the long axis of TnC is perpendicular to the thin filament without bound Ca^{2+}, and that TnC and the I-T arm tilt toward the filament axis and rotate around the Tm axis by ~20° upon Ca^{2+} binding.

Keywords: troponin; tropomyosin; fluorescence resonance energy transfer; muscle thin filament; Ca^{2+} regulation

**Corresponding author.* Division of Applied Chemistry and Biotechnology, Graduate School of Engineering Science, Fukui University, Fukui 910-8507, Japan. E-mail address: masao@acbio2.acbio.fukui-u.ac.jp.

† C.K.-S. and Y.U. contributed equally to this work.

Present address: C. Kimura-Sakiyama, ERATO Maéda Actin-filament Dynamics Project c/o RIKEN Harima Institute 1-1-1 Kouto, Sayo-gun, Hyogo 679-5148, Japan.

Abbreviations used: Tn, troponin; Tm, tropomyosin; FRET, fluorescence resonance energy transfer; S1, myosin subfragment-1; TnT25k, TnT 25-kDa fragment; DABMI, 4-dimethyl-aminophenylazophenyl 4′-maleimide; IAEDANS, 5-(2-iodoacetylaminoethyl) aminonaphthalene 1-sulfonic acid; AEDANS, IAEDANS attached to cysteine residue.

Introduction

The cyclic interaction of actin and myosin coupled with ATP hydrolysis generates the mechanical force in cell movements. In skeletal and cardiac muscles, this process is regulated by tropomyosin (Tm) and troponin (Tn) on the actin filament, in response to a change in Ca^{2+} concentration from approximately 10^{-7} to 10^{-5} M.[1–3] Rabbit skeletal muscle α-Tm is a 284-residue dimeric coiled-coil protein. It contains seven quasiequivalent regions and spans seven actin monomers along the two-start long-pitch helix of F-actin.[4] Tn is an elongated complex of three proteins: TnC, TnI and TnT. TnI inhibits the actin–myosin interaction, and TnC suppresses the inhibitory effect of TnI by binding Ca^{2+}. TnT binds to Tm and integrates the whole Tn complex into the thin filament. TnT is divided into two regions at residue 159: TnT1 and TnT2.[5] TnC, TnI and the C-terminal part of TnT (TnT2) constitute the globular portion of the Tn complex, which is located near residues 150–180 of Tm.[6] The elongated N-terminal part of TnT (TnT1) extends along the C-terminal region of Tm to the beginning of the next Tm molecule on the actin filament.[7]

Fluorescence resonance energy transfer (FRET) spectroscopy is an optical ruler for measuring the distance in the range of 10–70 Å. This method has been extensively applied in structural studies of muscle proteins.[8] Due to the ambiguity in the value of the dipole–dipole orientation factor between the energy donor and acceptor molecules and to the dimensions of the probes attached by linkers to the side chains of the amino acid residues, the measured distance will have an uncertainty of ±10%.[8] Using the observed intramonomer FRET efficiencies of actin, we constructed a FRET model of the actin monomer in which the deviation in transfer efficiencies was minimized by using a computer algorithm.[9] Furthermore, the FRET-modeled actin monomer was oriented within a filament by use of the intermonomer FRET efficiencies.[8,9] In spite of the uncertainty derived from the orientation factor and the probe size, the FRET model was in good agreement with the atomic model of the actin filament.[10] FRET is an especially valuable method for detecting conformational changes, since the transfer efficiency is a function of the inverse of the sixth power of the distance between probes.[11] FRET between probes attached to TnI or TnT and actin showed a significant extent of Ca^{2+}- and myosin subfragment-1 (S1)-induced movements of TnI and TnT on the reconstituted thin filament.[12,13]

Recently, crystal structures of the Tn core domain have been solved for a human cardiac Tn[14] and a chicken skeletal Tn.[15] The Tn core domain has two characteristic subdomains: (1) the "regulatory head," composed of the N-terminal region of TnC and the C-terminal region of TnI, and (2) the "I-T arm," composed of long coiled-coil regions from TnT2, TnI and the C-terminal lobe of TnC. The relative orientation of the regulatory head and the I-T arm may play a fundamental role in the regulatory mechanism. However, many components of the regulatory machinery are missing from the crystal structure of the core complex, including parts of TnI and TnT, Tm and actin. The detailed positions of Tn subunits on the thin filament and their changes in response to the on and off states of the thin filament are not yet known. Several attempts have been made to locate the Tn core domain on the thin filament by searching for the best docking positions on bumps on the three-dimensional reconstruction model from electron microscopic images of thin filaments,[16,17] and by analyzing polarized fluorescence data from bifunctional rhodamine probes of TnC in muscle fibers.[18,19]

In the present study, we generated single-cysteine mutants of a rabbit skeletal α-Tm, TnI and the β-type TnT 25-kDa fragment (TnT25k), which has the same properties as the intact TnT.[20] We measured intermolecular FRET between probes attached to Tn subunits and Tm on the reconstituted thin filament and constructed a FRET model of the Tn–Tm complex in the presence and absence of Ca^{2+}. In order to place the atomic structure of the Tn core domain on Tm, a global search by rigid-body movements of the crystal structure was carried out to find the position and orientation at which the deviations between the calculated and observed FRET efficiencies were minimized. For experiments both with and without bound Ca^{2+}, the best-fit models were obtained, in which the Tn core domain is located on residues 160–200 of Tm. We propose models of the Tn core domain and Tm complex in the thin filament and also discuss a Ca^{2+}-induced change in the orientation of the Tn core domain on Tm. These models could be useful for constructing a thin filament model by using FRET data between probes attached to the Tn subunits or Tm and F-actin.

Results and Discussion

To study the proximity between specific residues of Tn and Tm in the reconstituted thin filament and the changes in response to a change in Ca^{2+} concentration, FRET efficiencies between probes attached to the Tn subunits and Tm were measured in the presence and absence of Ca^{2+}. The energy donor molecule, 5-(2-iodoacetylaminoethyl) aminonaphthalene 1-sulfonic acid (IAEDANS), IAEDANS attached to cysteine residues (AEDANS) at positions 60, 73, 127, 159, 200 or 250 on TnT25k, and at 1, 9, 133 or 181 on TnI. The energy acceptor molecule, 4-dimethyl-aminophenylazophenyl 4′-maleimide (DABMI), was attached to each cysteine of the single-cysteine Tm mutants (13, 146, 160, 174, 190, 209, 230, 271 or 279). In the thin filament, TnT binds to Tm in an anti-parallel manner, and the tail domain exists as a partial α-helix elongated along Tm. The labeling positions in the present study are shown in Fig. 1. The residues at 60, 73 and 127 on TnT25k are included in the Tn tail domain, and the others are in the Tn globular domain. Low-resolution X-ray analysis of the co-crystal of Tn and Tm suggested

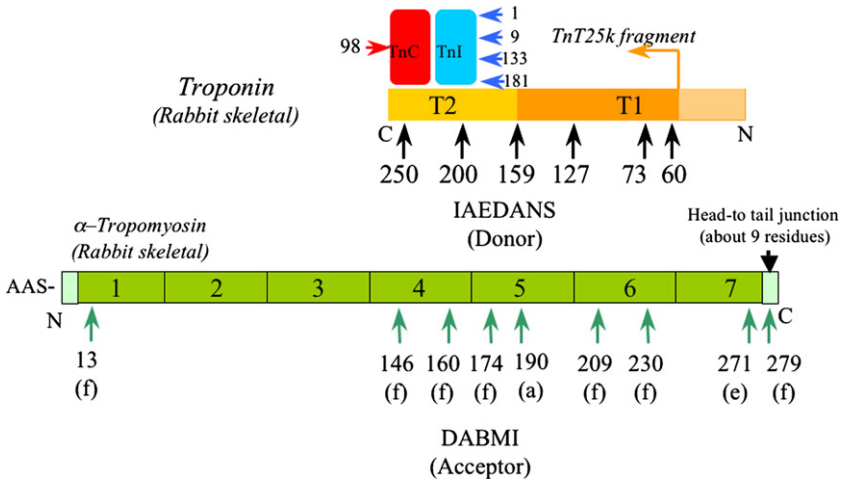

Fig. 1. A schematic representation of the Tn–Tm complex with the donor and acceptor labeling sites. Residues 1, 9, 133 or 181 in TnI, 98 in TnC and 60, 73, 127, 159, 200 or 250 in the TnT 25-kDa fragment (TnT25k) were selectively labeled with a donor molecule (AEDANS). Residues 13, 146, 160, 174, 209, 230, 271 or 279 in Tm were selectively labeled with an acceptor molecule (DABMI). The AEDANS-labeled Tn subunit was reconstituted with other nonlabeled components. The number of labeling sites on TnT25k was according to that of the full-length rabbit skeletal β-TnT.

that the Tn globular domain binds to Tm near residues 150–180.[6] The residues at 146, 160, 174 and 190 on Tm are in the vicinity of this Tn core domain-binding region. The residues at 209, 230, 271 and 279 are located on the C-terminus of Tm, and residue 13 is on the junction domain of the next Tm molecule.

ATPase activities of reconstituted thin filaments with labeled TnT25k and Tm mutants

To examine whether the AEDANS-labeled TnT25k mutants have the same function as native TnT, Ca^{2+} regulation of the actin-activated S1-ATPase activity with the Tn complex composed of the labeled TnT25k was measured. Measurements were performed at 25 °C in 10 mM KCl, 5 mM $MgCl_2$, 2 mM ATP, 20 mM Tris–HCl (pH 7.6), 1 mM DTT and either 50 μM $CaCl_2$ for the $+Ca^{2+}$ state or 1 mM ethylene glycol bis(β-aminoethyl ether) *N*,*N*′-tetraacetic acid (EGTA) for the $-Ca^{2+}$ state. Protein concentrations were 4 μM F-actin, 0.57 μM Tm, 0.67 μM Tn and 1 μM S1. The S1-ATPase activity in the absence of Tn and Tm was defined as 100% (0.9 s^{-1}). All experiments were carried out with the sample in the absence of Tn and Tm as a reference. The Tn complexes with these labeled TnT25k mutants indicated slightly lower activities than native rabbit skeletal Tn, but they had a Ca^{2+} sensitivity of more than 70%, where the Ca^{2+} sensitivity is defined as $\{1-(\text{Activity}_{-Ca}/\text{Activity}_{+Ca})\}\times 100$. ATPase measurements indicated that neither the mutation nor the labeling of AEDANS affected the regulatory activity of TnT (Fig. 2). Ca^{2+} sensitivities of DABMI-Tm mutants with Tn were also measured under the same conditions as AEDANS-labeled Tn (TnT25k). They had almost the same activity as native α-Tm, except for DABMI-Tm labeled at 160, which had a Ca^{2+} sensitivity of 54.4±17.3%.

FRET between Tm and the globular region of Tn on the reconstituted thin filament

TnI, TnC and the C-terminal region of TnT constitute the globular portion of Tn. FRET was measured between AEDANS attached to Cys200 or Cys250 of TnT25k and DABMI attached to Tm on the reconstituted thin filament. The overlap integral, *J*, was calculated to be $6.74\times10^{14}\ M^{-1}\ cm^{-1}\ nm^4$ for the AEDANS-Tn/DABMI-Tm pair. The quantum yield of Tn (TnT25k-200-AEDANS) was 0.28 both in the presence and in the absence of Ca^{2+}, and that of Tn (TnT25k-250-AEDANS) was 0.34 and 0.37 in the presence and absence of Ca^{2+}, respectively, as reported by Kimura *et al.*[13] Förster's critical distance, R_0, for the Tn (TnT25k-200-AEDANS)/DABMI-Tm pair was 37.5 Å. The critical distance for the Tn (TnT25k-250-AEDANS)/DABMI-Tm pair was 38.8 and 39.3 Å in the presence and absence of Ca^{2+}, respectively. The solvent condition for these experiments was 30 mM KCl, 2 mM $MgCl_2$, 20 mM Tris–HCl (pH 7.6), 1 mM NaN_3 (buffer F) and either 50 μM $CaCl_2$ for the $+Ca^{2+}$ state or 1 mM EGTA for the $-Ca^{2+}$ state at 20 °C. The ratio of donor fluorescence quenching was measured by titrating the AEDANS-Tn/actin with DABMI-Tm in the presence

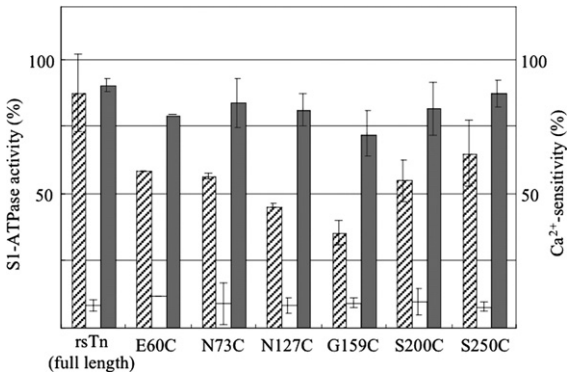

Fig. 2. Ca^{2+}-dependent regulation of acto-S1-ATPase by the labeled TnT25k. The reactions were carried out at 25 °C with 4 μM F-actin, 1 μM rabbit skeletal S1, 0.57 μM Tm and 0.67 μM Tn in 10 mM KCl, 5 mM $MgCl_2$, 1 mM DTT, 2 mM ATP and 20 mM Mops (pH 7.0) in the presence of 50 μM $CaCl_2$ (hatched bar graphs) or 1 mM EGTA (open bar graphs). The ordinate value of 100 (%) represents the ATPase activity of actoS1 without regulatory proteins under the same experimental conditions. The Ca^{2+} sensitivities defined as $\{1-(\text{Activity}_{-Ca}/\text{Activity}_{+Ca})\}\times 100$ were also shown (grey bar graphs).

and absence of Ca^{2+}, as described by Kimura *et al.*[13] The excitation wavelength was 340 nm and the emission was measured at 490 nm. For the correction of the fluorescence intensity change upon binding to Tm or due to dilution effects, the same amount of nonlabeled Tm was added to the AEDANS-Tn/actin solution, and the ratio of these fluorescence intensities was taken as the relative fluorescence intensity. The apparent decrease of the fluorescence intensity due to the inner effects arising from the absorption of DABMI-Tm was corrected according to Eq. (5) in Materials and Methods. The relative fluorescence intensity decreased with increasing molar ratio of Tm/Tn up to 1, and became almost constant above 1. The energy transfer efficiencies were obtained from the saturation points. In the case of a single donor and two acceptors, if the distances between the single donor on Tn and the acceptor attached to one α-chain (r_1) or another α-chain (r_2) of Tm are the same, then the distance can be calculated from Eq. (6) in Materials and Methods using values of the transfer efficiency, R_0 and the labeling ratio of DABMI to Tm. FRET efficiencies between AEDANS attached to Cys1, Cys9, Cys133 or Cys181 of TnI and DABMI attached to Tm were also measured under the same solvent conditions and in the same way as for AEDANS-TnT. The results are summarized in Table 1. FRET data indicated that TnT200 was located relatively far away from the Tm molecule and that TnT250 was close to residues 146–190 of Tm. Residues 1, 9 and 133 of TnI were close to residues 160 and 174 of Tm, and these distances changed significantly in response to a change in the Ca^{2+} concentration. On the other hand, residue 181 of TnI was relatively far from Tm.

FRET between the tail region of Tn and Tm on the reconstituted thin filament

FRET efficiencies between AEDANS attached to residues 159, 127, 73 or 60 of TnT25k and DABMI attached to Tm were measured in the same way as was mentioned above for TnT200 and TnT250. Rabbit skeletal TnT can be split into two subfragments, TnT1 (1–158) and TnT2 (159–259), by mild treatment with chymotrypsin.[5] The α-helical region of residues 71–150 (called the CB2 fragment) forms a stable triple-stranded binding structure with the coiled-coil Tm.[22,23] The N-terminal residue 159 of TnT2 is likely to be located at the junction region between the core domain and the rod portion of TnT. These results are summarized in Table 2. These transfer efficiencies were not sensitive to Ca^{2+} concentration, in contrast to FRET between the globular portion of Tn and Tm. The FRET efficiency between residue 60 of TnT and the N-terminal residue 13 of Tm was higher than that between residue 60 of TnT and the C-terminal residue 279 of Tm, suggesting that the N-terminal residue 60 of TnT is located beyond the head-to-tail region of Tm. Residue 127 in TnT, which is located in the middle part of TnT1, was very close to Tm230. The number of residues between residues 60 and 127 in TnT is nearly equal to the number of residues between residue 230 in Tm and residue 13 in the next Tm. This suggests that the tail region in TnT, residues 60–127, extends as an α-helix along the α-helical coiled-coil of Tm over the N-terminal region of the next Tm molecule. This is in accordance with the report that a troponin T fragment, Gly-hcTnT70–170 stabilizes an overlap

Table 1. FRET between Tm and the globular region of Tn on the reconstituted thin filament

	Q		R_0 (Å)		Tm		Efficiency		$r_1 = r_2$ (Å)	
Tn donor	+Ca	−Ca	+Ca	−Ca	acceptor	A/P[a]	+Ca	−Ca	+Ca	−Ca
TnT200	0.28		37.5		146	2.0	0.16±0.05	0.13±0.07	55.5	57.8
					160	2.0	0.19±0.05	0.14±0.05	53.6	57.0
					174	2.0	0.27±0.03	0.22±0.04	49.7	52.0
					190	2.0	0.34±0.03	0.16±0.05	47.0	55.5
TnT250	0.34	0.37	38.8	39.3	146	2.0	0.42±0.02	0.50±0.01	46.0	44.1
					160	2.0	0.56±0.05	0.69±0.05	41.8	38.6
					174	2.0	0.57±0.05	0.77±0.01	41.6	36.1
					190	2.0	0.57±0.03	0.78±0.03	41.6	35.7
TnC98[b]	0.25	0.23	37.5	37.0	190[b]	1.4	0.18±0.02	0.10±0.02	50.7	56.2
TnI1	0.36	0.35	39.4	39.2	146	2.0	0.30±0.04	0.37±0.03	50.9	48.1
					174	2.0	0.29±0.02	0.41±0.03	51.4	46.8
					190	2.0	0.16±0.03	0.30±0.02	58.3	50.7
TnI9	0.33	0.31	38.8	38.4	146	2.0	0.28±0.04	0.33±0.03	51.0	48.5
					160	2.0	0.13±0.04	0.46±0.04	59.8	44.2
					174	2.0	0.23±0.03	0.45±0.09	53.2	44.5
					190[b]	1.4	0.12±0.02	0.20±0.02	57.0	50.7
TnI133	0.27	0.30	37.5	38.2	146	2.0	0.12±0.04	0.29±0.04	58.7	49.7
					160	2.0	0.20±0.04	0.41±0.04	53.0	45.6
					174	2.0	0.29±0.03	0.39±0.02	48.8	46.2
					190[b]	1.4	0.14±0.02	0.16±0.02	53.4	52.9
TnI181	0.27		37.5		146	2.0	0.12±0.03	0.18±0.02	58.7	54.2
					160	2.0	<0.05	0.1	>69	60.7
					174	2.0	0.17±0.03		54.5	
					190	2.0	0.10±0.01	0.15±0.02	60.7	56.2

[a] A/P, labeling ratio of DABMI to Tm.
[b] Data from Hai *et al.*[21]

Table 2. FRET between Tm and the tail region of Tn on the reconstituted thin filament

Donor (Tn)	Q +Ca	Q −Ca	R_0 (Å) +Ca	R_0 (Å) −Ca	Acceptor (Tm)	A/P	Efficiency +Ca	Efficiency −Ca	$r_1=r_2$ (Å) +Ca	$r_1=r_2$ (Å) −Ca
TnT60	0.26	0.30	36.9	37.7	230	2.0	0.37±0.02	0.24±0.01	45.3	51.3
					271	2.0	0.70±0.03	0.66±0.02	36.0	37.9
					279	2.0	0.56±0.02	0.67±0.03	39.8	37.6
					13	2.0	0.84±0.05		31.4	32.1
TnT73	0.29		37.4		230	2.0	0.34±0.03	0.29±0.02	46.8	48.7
					271	2.0	0.82±0.02		32.6	
					279	2.0	0.74±0.03		35.3	
					13	2.0	0.86±0.05		31.0	
TnT127	0.27		36.1		190	2.0	0.13±0.02		55.6	
					230	2.0	0.92±0.02		27.0	
TnT159	0.39		39.5		190	2.0	0.50±0.02		44.3	
					209	1.7	0.70±0.03		36.8	

complex of N-terminal and C-terminal tropomyosin molecules.[7]

Figure 3 shows the values of f/f_0 (=1−E) for residues 9 or 133 of TnI and residues 60, 73, 200 or 250 of TnT against the residue number of Tm. The value f/f_0 is related to the distance between probes on Tn and Tm. The results indicate that the globular portion of Tn is located near residues 146–190 of Tm, in accordance with the results of X-ray analysis of co-crystals of Tm and Tn, in which the Tn globular portion was located near residues 150–180.[6]

Determination of the orientation of the Tn core domain on Tm

The sizable amount of data on FRET efficiencies between probes attached to the Tn core domain and Tm has been collected from the present measurements and the previous report by Hai *et al.*[21] Since

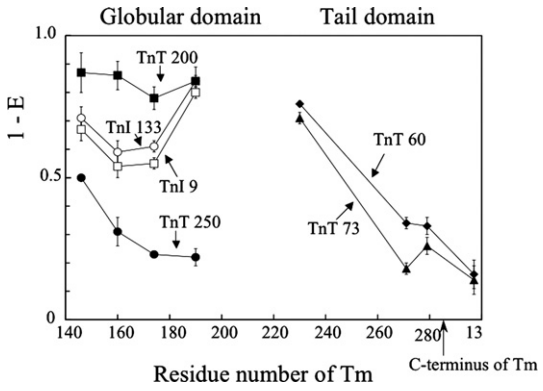

Fig. 3. The energy transfer efficiencies between TnT or TnI-AEDANS and Tm-DABMI in the absence of Ca^{2+} *versus* the residual numbers of Tm. The filled circle (●), square (■), triangle (▲) and diamond (♦) indicate the efficiencies of TnT250, 200, 73 and 60, respectively. The open circle (○) and square (□) indicate those of TnI133 and 9, respectively. TnT250 and 200 and TnI133 and 9 are included in the Tn globular domain. TnT73 and 60 are located at the end of the Tn tail domain (composed of TnT25k). Rabbit skeletal α-Tm has 284 amino acid residues and forms an α-helical coiled coil over the whole molecule. TnT and Tm bind in an anti-parallel manner. The FRET between Tm13 and TnT60 or TnT73 could occur from the next Tm.

several sites of these probes are included in the atomic structure of the Tn core domain, we attempted to place the atomic structure of the Tn core domain on Tm using the distance information derived from these FRET data. As mentioned in Materials and Methods, the atomic model of the pig skeletal Tm (PDB ID code 1C1G) was fixed along the *z*-axis from the C-terminus to the N-terminus, on which two energy acceptor molecules (DABMI) resided. Once the atomic model of the chicken skeletal Tn core domain (PDB ID code 1YTZ) was placed on Tm with rigid-body movement, two distances between the donor and two acceptors were obtained for each FRET pair. Then, the energy transfer efficiency between the positions of the sites on the Tn and Tm molecules for each FRET pair was calculated according to Eq. (7) in Materials and Methods, where the C^{α} coordinates of the labeled amino acid residues were used as the label positions. Through translation and rotation of the Tn core domain, the goodness of fit of the model was evaluated by the squared sum of deviations of the calculated energy transfer efficiencies from the observed values (Table 1) instead of a comparison of the FRET distances (see Materials and Methods), since the value measured from FRET is not the distance, but rather the transfer efficiency. The model with the lowest residual value of the squared sum was derived in a parameter space by means of a global minimum search for each set of FRET data in the presence and absence of Ca^{2+}. For every Eulerian angle as a rotational parameter, the optimal disposition of the Tn core domain was searched with a step size variation of 3 Å throughout the range of ±60 Å translations of *x*, *y* and *z*. Then, each fitting residual was listed, and by sorting the lowest residual values calculated from all orientations, the global minimum and corresponding Eulerian angles were determined. The trend of fitting residuals in terms of orientations were examined in the residual map in a 10° grid for each of two Eulerian angles, α and β, among various values of the third angle, γ (Fig. 4). Because the labels on Tm primarily sit close to the *z*-axis, whose *x* and *y* coordinates are close to zero, any rotation around the *z*-axis was less sensitive to the fitting residual, but an appropriate rotation increased the fitness of the FRET data. There-

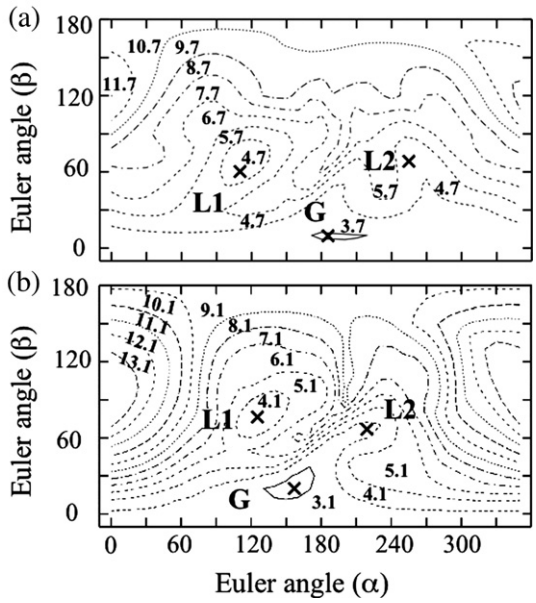

Fig. 4. A residual map of calculated FRET efficiency against the observation for each orientation of the Tn core domain in the presence (a) and absence (b) of Ca^{2+}. For each Eulerian angle of α and β, the minimum residuals in the series of the third Eulerian angle, γ, and translation parameters (x, y and z) are displayed as two-dimensional maps. There is a global minimum, G, and two local minimums, L1 and L2. The numbers on the contour line indicate the residual values.

fore, the orientation of the model is basically described by α and β, and the global minimum in the residual map in terms of α and β was confirmed as giving the best-fit model.

A model for the +Ca^{2+} state

Figure 4a shows the residual map of the calculated FRET efficiencies for the orientation of the Tn core domain in the presence of Ca^{2+}. Two local minimums appeared (L1 and L2) in addition to the global minimum (G), and the local minimums showed a tendency to fall into the valley of the global minimum. The appearance of local minimums might be partly due to an overfitting of inappropriate models to the FRET data. In these models of L1 and L2 in Fig. 4a, the Tn core domain sits too close to Tm to participate in a reasonable molecular interaction with Tm. In addition, in the L1 model, the H2(T2) and H2(I) helices of the I-T arm in the Tn core domain pass through the space between the α-helical coiled coils of Tm. Thus, these local minimum models are unrealistic.

Figure 5 shows the model for the global minimum (G) in Fig. 4a as the best-fit orientation of the Tn core domain in the presence of Ca^{2+}. The arrowhead-shaped I-T arm tilts by ~45° to the Tm axis, and its pointed end points toward the C-terminus of the Tm molecule. The angle between TnT-H2 (amino acids 200–244) and Tm was ~45°, that between TnI-H2 (amino acids 56–96) and Tm was ~51°, and the angle between the long axes of TnC and Tm was calculated to be ~75°.

The overall rms error between the calculated transfer efficiencies and observed values was 0.139. The comparison of the individual FRET efficiency of the model to the observed data is shown in Table 3.

The deviations of some calculated values were greater than the standard deviation obtained from FRET measurements. Major deviations were in the pairs with TnT200, in which the observed transfer efficiencies were significantly greater than the calculated values. Any improved fits to those transfer efficiencies caused unfavorable deviations for other data. In the present calculation, the transfer efficiencies were calculated between one donor on the Tn core domain and two acceptors on one Tm molecule. However, the FRET efficiencies were measured in the reconstituted thin filament. In order to take the Tm molecule on the opposite side of the filament into account, the transfer efficiencies should be calculated between one donor on the Tn core domain and four acceptors on two Tm molecules. From the analysis of the three-dimensional recon-

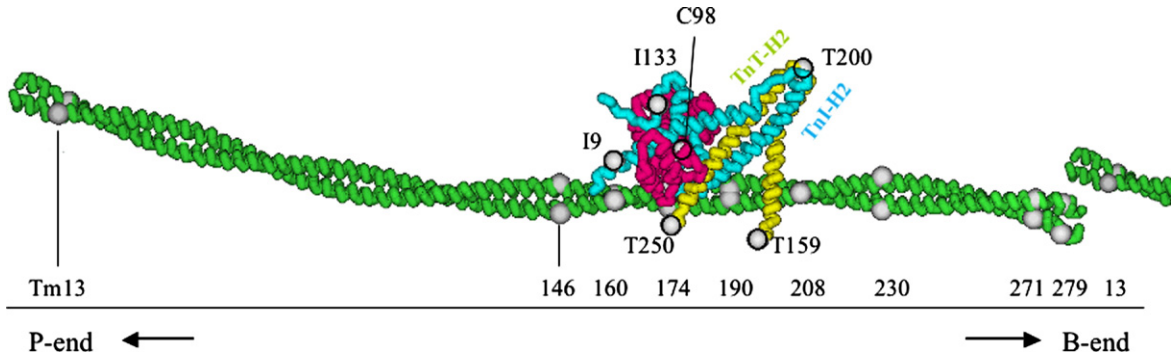

Fig. 5. The best-fit model of Tm and the Tn core domain complex in the presence of Ca^{2+}. Atomic models of the chicken skeletal Tn core domain (PDB code 1YTZ) and pig skeletal Tm (PDB code 1C1G) are depicted with alpha-carbon backbone models. TnC is in red, TnI in light blue and TnT in yellow. Large spheres indicate the residues labeled by a FRET donor or acceptor. In this view, the C-terminal lobe of TnC is underneath the N-terminal lobe. There should be partial C-terminal fragments missing in the crystallographic model for both TnI and TnT, which are close to TnC. The N-terminal part of TnT runs toward the C-terminal end of Tm.

Table 3. The observed and calculated transfer efficiencies in the best-fit model

		$+Ca^{2+}$				$-Ca^{2+}$			
Donor site	Acceptor site	E_{obs}	E_{calc}	r_1 (Å)	r_2 (Å)	E_{obs}	E_{calc}	r_1 (Å)	r_2 (Å)
TnC98	Tm190	0.18	0.13	53.9	54.1	0.10	0.15	51.1	52.8
TnT159	Tm190	0.50	0.64	39.0	41.9	0.50	0.62	40.3	41.2
	Tm209	0.70	0.62	35.6	46.4	0.70	0.63	35.1	46.8
TnT200	Tm146	0.16	0.00	111.2	113.8	0.13	0.00	109.4	115.4
	Tm160	0.19	0.01	93.8	98.1	0.14	0.01	96.9	97.6
	Tm174	0.27	0.02	76.2	85.6	0.22	0.02	79.7	88.4
	Tm190	0.34	0.06	66.4	68.0	0.16	0.04	71.6	74.7
TnT250	Tm146	0.42	0.16	55.1	61.2	0.50	0.22	53.5	55.6
	Tm160	0.56	0.52	39.6	50.6	0.69	0.70	35.3	45.1
	Tm174	0.57	0.67	36.6	42.5	0.77	0.90	27.8	38.4
	Tm190	0.57	0.47	43.3	45.5	0.78	0.69	38.4	39.0
TnI133	Tm146	0.12	0.09	61.1	63.9	0.29	0.15	54.3	62.3
	Tm160	0.20	0.23	48.9	56.1	0.41	0.32	48.4	48.5
	Tm174	0.29	0.36	42.6	55.3	0.39	0.47	40.6	50.7
	Tm190	0.14	0.12	54.2	55.5	0.16	0.16	51.8	54.6
TnI9	Tm146	0.28	0.14	57.7	60.6	0.33	0.39	45.0	48.7
	Tm160	0.13	0.24	49.1	60.9	0.46	0.51	40.3	47.5
	Tm174	0.23	0.17	53.1	63.5	0.45	0.35	44.1	55.3
	Tm190	0.12	0.04	68.8	69.4	0.20	0.06	63.5	64.5

r_1 and r_2 are the distances between one donor on Tn and two acceptors on Tm in the best-fit model. The rms error and Eulerian angles (α, β and γ) are 0.139, 200, 10 and 170, respectively, for $+Ca^{2+}$ and 0.123, 150, 20 and 190, respectively, for $-Ca^{2+}$ in the best-fit model.

structions of electron microscopic images of the reconstituted thin filament, the Tm molecules are positioned at a radius of 38 Å.[24] A Tm molecule on an actin filament is ~70 Å apart from the position of the Tm molecule on the opposite side. Since the transfer efficiency is a function of the inverse of the sixth power of the distance between donor and acceptor probes, the acceptors on the opposite Tm molecule would not affect the transfer efficiencies for the residues on the Tn core domain located near the Tm molecule, such as TnT250 and TnT159 (see Fig. 5). However, a residue such as TnT200, which projects far from the Tm molecule, may be located close to the acceptors on the opposite Tm molecule in the filament. Indeed, performing the calculation with one donor and four acceptors significantly improved the fit for the TnT200 efficiencies. However, in this calculation, the geometric constraint excluding a collision of the Tn core domain with F-actin was not included. At the present time, there are not enough FRET data between points on the Tn core domain and actin to place the Tn–Tm model on an F-actin filament; thus, we did not attempt such a calculation with one donor and four acceptors on a thin filament. The present Tn–Tm model could be greatly improved by making a thin filament model. Recently, two models for the orientation of the Tn core domain on the thin filament have been reported from the three-dimensional image reconstruction analysis of electron micrographs,[16,17] in which the orientations of the Tn core domain against the pointed end of the thin filament are different from each other. The present model is compatible with the orientation of the model by Pirani *et al.*[17]

A similar search was also performed for the model by using the atomic structure of the human cardiac Tn core domain (PDB ID code 1J1E). Although its structure is nearly identical with the structure of the skeletal Tn core domain, the N-terminal residue of TnT fragment in the crystal structure, 202 (177 in the rabbit skeletal TnT sequence), is far apart from TnT159. Therefore, the coordinate for TnT159 is not available, so the FRET data with TnT159 could not be used for evaluation of the fitness of the model. Furthermore, TnI133 of cardiac Tn also has a different coordinate from the skeletal Tn. The search often revealed a global minimum at a different locus in the residual map, where it was very close to the local minimum L2 found in the case of skeletal Tn. However, such a model seems to be unrealistic, because TnT159 would interfere with Tm if it were on the helix extending to the C-terminal side of TnT2 in the cardiac model. The simulation without the coordinate of TnT159 did not result in a realistic model. Thus, TnT159 is an indispensable residue in determining the orientation of the Tn core domain on Tm.

A model for the $-Ca^{2+}$ state

The crystal structure of the Tn core domain in the absence of Ca^{2+} (PDB ID code 1YV0) is missing several segments (159–163 in TnT, 119–143 in TnI and 86–95 in TnC) compared with the crystal structure in the presence of Ca^{2+} (1YTZ). Thus, the simulation with this structure (1YV0) could not lead to a proper best-fit model since the indispensable residue TnT159 was missing. However, the overall structure of 1YV0 is almost identical with that of 1YTZ. Therefore, by using 1YTZ instead of 1YV0 and the FRET data in the absence of Ca^{2+}, the best-fit orientation of the Tn core domain on Tm without bound Ca^{2+} was searched in the same way as in the case with bound Ca^{2+}. The fitting residual map (Fig. 4b) showed a global minimum, as in the case of the $+Ca^{2+}$ state. Figure 6 shows the best-fit model obtained from the global minimum in Fig. 4b in the absence of Ca^{2+} (blue), superimposed on that in the

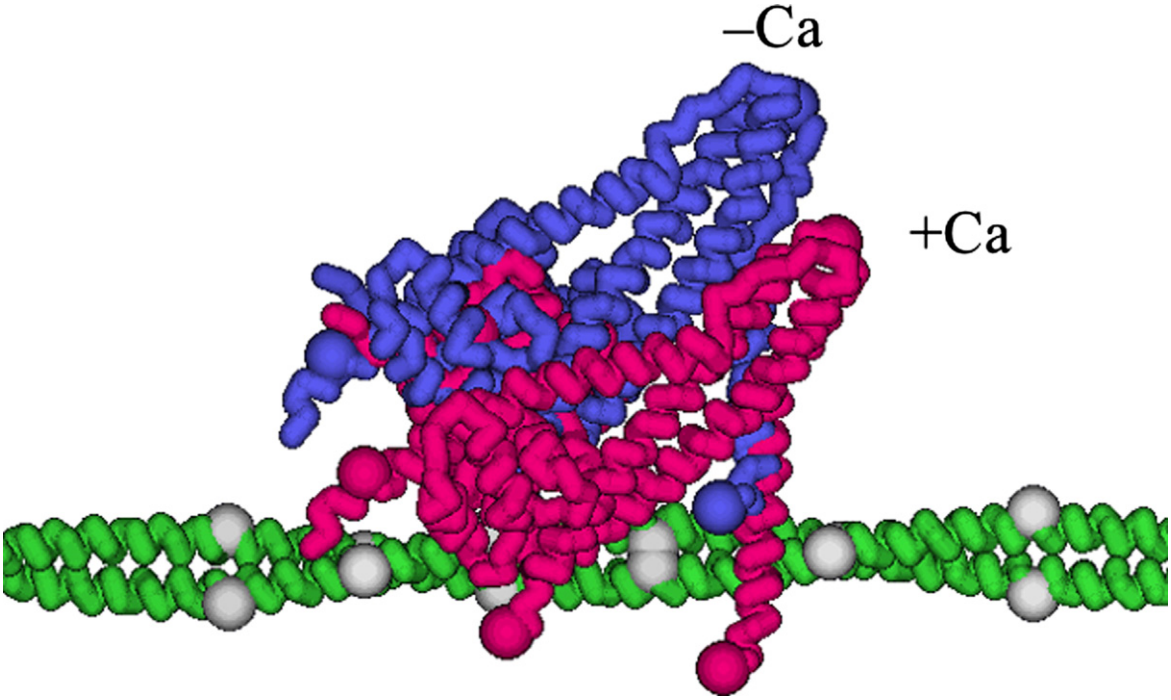

Fig. 6. The best-fit models of the Tn core domain and Tm complex in the presence (red) and absence (blue) of Ca^{2+}. Each best-fit model is superimposed with the orientation of tropomyosin coincident. The pointed end of the actin filament is towards the left.

presence of Ca^{2+} (red). The overall rms error was 0.123, which was smaller than in the case with bound Ca^{2+}. The comparison of the individual FRET efficiency of the model to the observed data is also shown in Table 3. The model showed a slight but significant change in the orientation of the Tn core domain on the Tm molecule. The angle between the long axes of TnC and Tm was ~85°, greater by ~10° than that in the case with bound Ca^{2+}, while the angles between the axes of Tm and TnT-H2 or TnI-H2 were ~54° and ~56°, respectively, greater by ~10° or ~5° than those in the case with bound Ca^{2+}. Overall, the arrowhead-shaped I-T arm rose up on Tm upon releasing Ca^{2+}. Furthermore, the Tn core domain rotated around the Tm axis by ~20° compared to the case of the $+Ca^{2+}$ state, consistent with previous reports from FRET measurements between probes attached to Tn and F-actin in which the globular portion of Tn moves around the axis of Tm toward the outer domain of actin in the filament upon releasing Ca^{2+}.[12,13,25] The results show that distinct changes in the orientation of the Tn core domain on Tm occur upon releasing Ca^{2+}.

Large FRET efficiency changes in the pairs with TnI133 upon releasing Ca^{2+} were not well explained in this modeling study solely by orientation or translation, while relatively small changes for the other sites could be well explained. TnI133 is located in the missing segment in the Ca^{2+}-free crystal structure 1YV0. The results suggest that the Tn core domain on the thin filament does not significantly change the bulk structure upon releasing Ca^{2+}, as shown in the comparison of the two crystal structures.[15] Instead, the results imply that the missing segments in 1YV0 (especially the mobile domain 131–182 of TnI) show a large Ca^{2+}-induced conformational change on the thin filament, which is assumed to be important for a switching mechanism of Ca^{2+} activation.

The angle between the Tm axis and the long axis of TnC was ~75° and ~85° in the presence and absence of Ca^{2+}, respectively. Since the angle between the thin filament axis and the Tm axis is ~27°, the angle between the thin filament axis and the long axis of TnC depends on the rotation of the Tn core domain around the Tm axis on the actin filament. Even though the precise angle between the TnC and the thin filament axes cannot be determined without placing the Tn–Tm complex on the actin filament, our present model suggests the following results: (1) the long axis of TnC orients close to perpendicularly to the thin filament axis in the absence of Ca^{2+}, and it tilts toward the filament axis by binding Ca^{2+}, in accordance with the previous reports;[18,19,26] (2) the arrowhead-shaped I-T arm tilts further toward the filament axis upon Ca^{2+} binding; and (3) the Tn core domain rotates around the Tm axis by ~20° further from the actin surface upon Ca^{2+} binding.

The present article has shown that the Tn core domain crystal structure can be oriented on Tm using FRET data between sites on Tn and Tm, and that the orientations of the TnC axis and the arrowhead-shaped I-T arm were altered by binding Ca^{2+}. Such orientational alterations of the Tn core domain on Tm would be responsible for Ca^{2+} regulation of thin filaments. Refined construction of a thin filament model from the FRET data between the

Tn core domain and F-actin could allow for the determination of the detailed conformational change of the Tn–Tm complex on the thin filament during the transition from the $-Ca^{2+}$ to $+Ca^{2+}$ states, which reveals the regulation mechanism of striated muscle contraction.

Materials and Methods

Reagents

IAEDANS and DABMI were purchased from Molecular Probes. All other chemicals were of analytical grade.

Protein preparations

Actin, S1 and Tn were prepared from rabbit skeletal muscle by the procedures of Spudich and Watt,[27] Weeds and Taylor[28] and Ebashi *et al.*,[29] respectively.

Construction of single-cysteine TnT25k, TnI and Tm mutants

A recombinant 25-kDa fragment of TnT (TnT25k), the sequence of which is based on the rabbit fast skeletal muscle β-TnT, lacks 58 amino acid residues at the N-terminus. The numbering of the amino acid sequence in the mutants is the same as that in the full-length TnT, beginning with residue 59 and ending at residue 266. In the present study, we prepared six single-cysteine TnT25k mutants TnT25k-E60C, N73C, N127C, G159C, S200C and S250C. TnT25k-E60C and TnT25k-S250C were constructed as previously reported by Kimura *et al.*[13] The mutagenesis for the other mutants was carried out on a pUC119 template cloned with a full-length wild-type β-TnT cDNA using the site-directed mutagenesis kit Mutan K (Takara Bio Co.), according to the manufacturer's protocol. The oligonucleotides for mutagenesis were as follows: GAGGT CCTTGCACTGCCGCTTC for N73C, CCGCCAGTCTGCACTGCCGCTCCC for N127C, CTGTAGTTGGCGCACATGGAG GAC for G159C and GCTTCTCGT CGCACAGGTGGTCG for S200C. To construct pTrc expression plasmids encoding TnT25k mutants, AccI–EcoRI fragments from the mutated pUC plasmids were inserted into pTrc99c between the NcoI and EcoRI sites, together with a pair of 14-bp oligonucleotides that filled in the gap between the NcoI and AccI sites. TnT25k mutants were expressed in AD202 cells and purified by passing through a Q-Sepharose fast-flow column (Pharmacia LKB Biotechnology, 2.5×10 cm) and a CM-Toyopearl 650 M column (Toso, 2.5×10 cm), as reported by Kimura *et al.*[13]

We prepared three single-cysteine TnI mutants (G1C, A9C and S181C) by undertaking mutagenesis of a cDNA encoding a Cys-less TnI mutant (C48A, C64A and C133S) as previously reported by Shitaka *et al.*[30] and Hai *et al.*[21] The cDNAs were inserted into pET23d expression vector. TnI mutants were expressed in BL21 (DE3) cells and purified on a Q-Sepharose fast-flow column, an S-Sepharose column and a TnC affinity column as reported by Shitaka *et al.*[30]

We constructed nine single-cysteine Tm mutants (L13C, I146C, R160C, S174C, I190C, A209C, D230C, S271C and N279C) based on the sequence of rabbit skeletal α-Tm. Template cDNA included extra oligonucleotides encoding Ala-Ala-Ser at the N-terminus of Tm, in which cysteine 190 was substituted by isoleucine.[31] The addition of three amino acid residues at the N-terminus substitutes for acetylation and restores actin-binding ability.[32] Site-directed mutagenesis was carried out by oligonucleotide-directed mutagenesis.[33] NdeI and BamHI fragments from the resultant plasmids were inserted into the pET23a expression vector. Tm mutants were expressed in BL21 (DE3) cells and purified by passing through a Q-Sepharose fast-flow column (Pharmacia LKB Biotechnology, 2.5 cm×10 cm) and a Cellulofine GCL-90-sf column (Seikagaku Corporation, 2.5 cm×10 cm) as reported by Kluwe *et al.*[34] The oligonucleotides used for mutagenesis were synthesized and purified by Invitrogen Life Technologies. The sequences of all mutants were confirmed by the use of DNA sequencing (ABI Genetic Analyzer 310). DNA sequencing was performed using the ABI PRISM 377 DNA sequencing system (ABI PRISM BigDye Terminator Cycle Sequencing Ready Reaction Kit, Applied Biosystems). We used the M13 (−21) control primer or other specific primers as appropriate, which were synthesized based on pTrc99C or pET23a promoter sequences.

Protein concentrations were determined from the absorbance using the following extinction coefficients (0.1%): $A_{290}=0.63\ cm^{-1}\ (mg/ml)^{-1}$ for G-actin, $A_{280}=0.75\ cm^{-1}$ for S1, $0.24\ cm^{-1}$ for Tm and Tm mutants, and $A_{280}=0.44\ cm^{-1}$ for Tn (TnT25k). Relative molecular masses of 42 kDa for actin, 115 kDa for S1, 66 kDa for Tm and Tm mutants and 64 kDa for Tn (TnT25k) were used.

Labeling of proteins

Labeling of mutant Tm at the cysteine residue with DABMI was carried out as follows. The Tm mutant (1 mg/ml) was mixed with a 50-fold molar excess of DABMI in 40 mM Tris–HCl (pH 8.0), 1 mM EDTA and 1 M KCl, and kept overnight at 25 °C. The reaction was terminated by the addition of 1 mM DTT, and the sample solution was extensively dialyzed against 10 mM Tris–HCl (pH 8.0) and 1 mM DTT to remove free DABMI. Labeling of the cysteine residues of TnT25k and TnI mutants with IAEDANS and the reconstitution of ternary Tn complexes with AEDANS-labeled TnT25k or TnI mutants were carried out as previously reported by Kimura *et al.*[13] and Shitaka *et al.*[30] The labeling of Cys133 of TnI was carried out by using native Tn as previously reported by Hai *et al.*[12] The absorption coefficients of 24,800 M^{-1} at 460 nm for DABMI[35] and 6100 M^{-1} at 337 nm for IAEDANS[36] were used for the determination of the labeling ratios.

The biochemical activity of the labeled Tn (TnT25k) and Tm was assayed by Ca^{2+}-dependent regulation of acto-S1 ATPase activity. Measurements were performed at 25 °C in 10 mM KCl, 5 mM $MgCl_2$, 2 mM ATP, 20 mM Tris–HCl (pH 7.6), 1 mM DTT and either 50 μM $CaCl_2$ for the $+Ca^{2+}$ state or 1 mM EGTA for the $-Ca^{2+}$ state. The protein concentrations used were 4 μM F-actin, 0.57 μM Tm, 0.67 μM Tn and 1 μM S1. The amounts of inorganic phosphate released were determined colorimetrically according to the method of Tausky and Shorr.[37]

Absorption was measured with a Hitachi U2000 spectrophotometer. Steady-state fluorescence was measured with a Perkin Elmer LS50B or Hitachi F-4500 fluorometer. The temperature was maintained at 20 °C.

Fluorescence resonance energy transfer

The efficiency E of resonance energy transfer between probes was determined by measuring the fluorescence

intensity of the donor both in the presence (F_{DA}) and in the absence (F_{D0}) of the acceptor as given by

$$E = 1 - F_{DA}/F_{D0} \quad (1)$$

In the case of a single donor and either a single or multiple acceptors, the transfer efficiency is related to the *i*th donor–acceptor distance (r_i) and Förster's critical distance (R_0), at which the transfer efficiency is equal to 50%, by

$$\Sigma_i {R_0}^6/{r_i}^6 = (E^{-1} - 1)^{-1} \quad (2)$$

R_0 can be obtained (in nanometers) as

$${R_0}^6 = (8.79 \times 10^{-11}) n^{-4} \kappa^2 Q_0 J \quad (3)$$

where n is the refractive index of the medium (taken as 1.4), κ^2 is the orientation factor, Q_0 is the quantum yield of the donor in the absence of the acceptor, and J is the spectral overlap integral between the donor emission $F_D(\lambda)$ and acceptor absorption $\varepsilon_A(\lambda)$ spectra, which is defined by

$$J = \int F_D(\lambda)\varepsilon_A(\lambda)\lambda^4 d\lambda / \int F_D(\lambda) d\lambda \quad (4)$$

The quantum yield was determined by a comparative method using quinine sulfate in 1 M H_2SO_4 as the standard, which has an absolute quantum yield of 0.70.[38] κ^2 was taken as 2/3 for the calculation of distances. The decrease of the fluorescence intensity due to the inner filter effect was corrected with

$$F_{corr} = F_{obs} \times 10^{(A_{ex} \times A_{em})/2} \quad (5)$$

where A_{ex} and A_{em} are the absorption of the sample at the excitation and emission wavelengths, respectively.

Simulation of FRET efficiency

The atomic coordinates of 1YTZ in the PDB database entry for the core domain (+Ca^{2+} form) of the chicken fast skeletal Tn and 1C1G for the pig skeletal Tm (which has almost the same amino acid sequence as that of rabbit skeletal Tm) were used. Residues 143 to 206 of Tm were aligned on the *z*-axis, and the Tn core model was approached to fit on the Tm molecule by graphics software. From the multiple alignments of TnI and TnT from various species,[14] the difference in residue numbering between the chicken skeletal Tn and the rabbit skeletal Tn was examined in order to assign the labeling residues on the crystal structure. TnT159 of the rabbit skeletal Tn corresponds to TnT157 of the chicken skeletal Tn. However, TnT157 is missing in the crystal structure. The N-terminal residue of TnT in the crystal structure is TnT159, and its α carbon (C^α) is ≤7 Å apart from that of TnT157. Here, the coordinate of TnT159 in the crystal structure was used for TnT159 of the rabbit skeletal Tn. Thus, available FRET donor labeling coordinates for TnT159, TnT200, TnT250, TnC98, TnI9 and TnI133 were assigned to residues 159, 198 and 248 on TnT, 100 on TnC, and 9 and 133 on TnI in the crystal structure (1YTZ), respectively. FRET efficiencies have been calculated from the distances between the α carbon atoms of the labeled residues. Since there are two acceptors on Tm, their efficiencies were summed by taking into account the labeling ratio of acceptors. Tm was assumed to take an α-helical coiled-coil structure through the whole molecule. For the dual acceptor case with the labeling fraction α (when α = 1, the labeling ratio = 2 in the case of Tm), four possible configurations are considered (no acceptor on either site, two acceptors or one acceptor on one site). The fluorescence intensity (f) in the presence of acceptor is calculated as follows.[39]

$$f = f_0\{(1-\alpha)^2 + \alpha^2/(1 + R_0^6/{r_1}^6 + {R_0}^6/{r_2}^6) + \alpha(1-\alpha)/(1 + {R_0}^6/{r_1}^6) + (1-\alpha)\alpha/(1 + {R_0}^6/{r_2}^6)\} \quad (6)$$

where f_0 is the fluorescence intensity in the absence of acceptor. Since $f/f_0 = 1 - E$, the transfer efficiency E is related to the distances between one donor and two acceptors as follow.

$$E = 1 - \{(1-\alpha)^2 + \alpha^2/(1 + {R_0}^6/{r_1}^6 + {R_0}^6/{r_2}^6) + \alpha(1-\alpha)/(1 + {R_0}^6/{r_1}^6) + (1-\alpha)\alpha/(1 + {R_0}^6/{r_2}^6)\} \quad (7)$$

Orientation search for the Tn core domain on Tm

The atomic model of Tm was fixed along the *z*-axis in the direction from its C-terminus to the N-terminus. The average value of the *z*-axis coordinates of the α carbon atoms of Tm146, Tm174 and Tm190 was taken as zero. The crystal structure model of the Tn core domain was brought close to the Tm molecule by graphical software, and the initial orientation of the model was decided upon. Then, the crystal model was moved with rigid body translation and rotation. Eulerian angles (α, β, γ) were employed for a comprehensive description of rotational parameters in Cartesian coordinates. At every orientation, two distances between a donor and two acceptors were calculated for each FRET pair, where the C^α coordinates of labeled amino acid residues were used for labeling positions. By using these distance values, the energy transfer efficiency (E_{calc}) between the positions of the sites on the Tn and Tm molecules for each FRET pair was calculated according to Eq. (7). The squared sum (Res) of deviations of the calculated energy transfer efficiencies from the observed values (E_{obs}) for all FRET pairs was calculated as follows:

$$Res = \Sigma_{data\ set}(E_{obs} - E_{calc})^2 \quad (8)$$

Through rigid-body translation and rotation of the Tn core domain, the goodness of fit of the model was evaluated by Res values. Our simulation searched for the global minimum of the squared sum of the transfer efficiency in a parameter space consisting of six parameters without the additional geometric constraints. For every Eulerian angle parameter in a 10° grid (0° < α and γ < 360°, 0° < β < 180°), the optimal position was searched at step size intervals of 3 Å through the range of ±60 Å translations of x, y and z from the initial point. The best residual value was listed for each set of Eulerian angles, and by sorting the residual values calculated from all orientations, the global minimum and corresponding Eulerian angles were determined. The trends of fitting residuals in terms of orientations were examined in the residual map for two Eulerian angles, α and β, among variations in the third angle, γ, in the series of translations (see Fig. 4). We found that the orientation of the model is well described by α and β, and therefore the global minimum in the residual map of α and β in the series of γ was selected as giving the best-fit model for the FRET data set in the presence and absence of Ca^{2+}.

Acknowledgements

We thank Dr. Kayo Maeda of the Riken Harima Institute for her gift of the cDNA clones of rabbit skeletal β-TnT 25-kDa fragment, Cys-less TnI mutant (C48A, C64A and C133S) and α-Tm, and also for her kind support in carrying out mutagenesis. This study was supported in part by the Special Coordination Funds of the Ministry of Education, Culture, Sports, Science and Technology, Japan (to K.W. and M.M.), and also by a Grant-in-Aid for Scientific Research from the Ministry of Education, Science, Sports and Culture of Japan (to M.M.).

References

1. Ebashi, S., Endo, M. & Ohtsuki, I. (1969). Control of muscle contraction. *Q. Rev. Biophys.* **2**, 351–384.
2. Farah, C. S. & Reinach, F. C. (1995). The troponin complex and regulation of muscle contraction. *FASEB J.* **9**, 755–767.
3. Gordon, A. M., Homsher, E. & Regnier, M. (2000). Regulation of contraction in striated muscle. *Physiol. Rev.* **80**, 85–924.
4. Perry, S. V. (2001). Vertebrate tropomyosin: distribution, properties and function. *J. Muscle Res. Cell Motil.* **22**, 5–49.
5. Ohtsuki, I. (1979). Molecular arrangement of troponin T in the thin filament. *J. Biochem. (Tokyo)*, **86**, 491–497.
6. White, S. P., Cohen, C. & Phillips, G. N., Jr. (1987). Structure of co-crystals of tropomyosin and troponin. *Nature*, **325**, 826–828.
7. Palm, T., Graboski, S., Hitchcock-DeGregori, S. E. & Greenfield, N. J. (2001). Disease-causing mutations in cardiac troponin T: identification of a critical tropomyosin-binding region. *Biophys. J.* **81**, 2827–2837.
8. Miki, M., O'Donoghue, S. I. & dos Remedios, C. G. (1992). Structure of actin observed by fluorescence resonance energy transfer spectroscopy. *J. Muscle Res. Cell. Motil.* **13**, 132–145.
9. O'Donoghue, S. I. (1991). Structural interpretation of fluorescence resonance-energy transfer measurements. *Comput. Appl. Biosci.* **7**, 471–477.
10. Holmes, K. C., Popp, D., Gebhard, W. & Kabsch, W. (1990). Atomic model of the actin filament. *Nature*, **347**, 44–49.
11. Lakowicz, J. R. (1999). *Principles of fluorescence spectroscopy*, 2nd edit. Kluwer Academic/Plenum Publishers, New York.
12. Hai, H., Sano, K.-I., Maeda, K., Maéda, Y. & Miki, M. (2002). Ca^{2+}-induced conformational change of reconstituted skeletal muscle thin filaments with an internal deletion mutant D234-tropomyosin observed by fluorescence energy transfer spectroscopy: structural evidence for three states of thin filament. *J. Biochem. (Tokyo)*, **131**, 407–418.
13. Kimura, C., Maeda, K., Maéda, Y. & Miki, M. (2002). Ca^{2+}- and S1-induced movement of troponin T on reconstituted skeletal muscle thin filaments observed by fluorescence energy transfer spectroscopy. *J. Biochem. (Tokyo)*, **132**, 93–102.
14. Takeda, S., Yamashita, A., Maeda, K. & Maéda, Y. (2003). Structure of the core domain of human cardiac troponin in the Ca^{2+}-saturated form. *Nature*, **424**, 35–41.
15. Vinogradova, M. V., Stone, D. B., Malanina, G. G., Karatzaferi, C., Cooke, R., Mendelson, R. A. & Fletterick, R. J. (2005). Ca^{2+}-regulated structural changes in troponin. *Proc. Natl Acad. Sci. USA*, **102**, 5038–5043.
16. Murakami, K., Yumoto, F., Ohki, S., Yasunaga, T., Tanokura, M. & Wakabayashi, T. (2005). Structural basis for Ca^{2+}-regulated muscle relaxation at interaction sites of troponin with actin and tropomyosin. *J. Mol. Biol.* **352**, 178–201.
17. Pirani, A., Vinogradova, M., Curmi, P. M., King, W. A., Fletterick, R. J., Craig, R. *et al.* (2006). An atomic model of the thin filament in the relaxed and Ca^{2+}-activated states. *J. Mol. Biol.* **357**, 707–717.
18. Ferguson, R. E., Sun, Y.-B., Mercier, P., Brack, A. S., Sykes, B. D., Corrie, J. E. *et al.* (2003). *In situ* orientations of protein domains: troponin C in skeletal muscle fibers. *Mol. Cell*, **11**, 865–874.
19. Sun, Y. B., Brandmeier, B. & Irving, M. (2006). Structural changes in troponin in response to Ca^{2+} and myosin binding to thin filaments during activation of skeletal muscle. *Proc. Natl Acad. Sci. USA*, **103**, 17771–17776.
20. Fujita, S., Maeda, K. & Maéda, Y. (1992). Expression in *Escherichia coli* and a functional study of a β-troponin T 25 kDa fragment of rabbit skeletal muscle. *J. Biochem. (Tokyo)*, **112**, 306–308.
21. Hai, H., Miura, T., Kobayashi, T., Maéda, Y. & Miki, M. (2000). Conformational changes of the troponin–tropomyosin complex on F-actin observed by fluorescence resonance energy transfer measurements. *J. Fluoresc.* **10**, 193–201.
22. Jackson, P., Amphlett, G. W. & Perry, S. V. (1975). The primary structure of troponin T and the interaction with tropomyosin. *Biochem. J.* **151**, 85–97.
23. Nagano, K., Miyamoto, S., Matsumura, M. & Ohtsuki, I. (1981). Possible formation of a triple-stranded coiled-coil region in tropomyosin–troponin T binding complex. *J. Mol. Biol.* **141**, 217–222.
24. Xu, C., Craig, R., Tobacman, L., Horowitz, R. & Lehman, W. (1999). Tropomyosin positions in regulated thin filaments revealed by cryoelectron microscopy. *Biophys. J.* **77**, 985–992.
25. Miki, M. (2007). Conformational changes in reconstituted skeletal muscle thin filaments observed by fluorescence spectroscopy. *Adv. Exp. Med. Biol.* **592**, 111–123.
26. Fujiwara, S. & Matsumoto, F. (2007). Orientational information of troponin C within the thin filaments obtained by neutron fiber diffraction. *J. Mol. Biol.* **367**, 16–24.
27. Spudich, J. A. & Watt, S. (1971). The regulation of rabbit skeletal muscle contraction. I. Biochemical studies of the interaction of the tropomyosin–troponin complex with actin and the proteolytic fragments of myosin. *J. Biol. Chem.* **246**, 4866–4871.
28. Weeds, A. G. & Taylor, R. S. (1975). Studies on the chymotryptic digestion of myosin. Effects of divalent cations on proteolytic susceptibility. *Nature*, **257**, 54–56.
29. Ebashi, S., Wakabayashi, T. & Ebashi, F. (1971). Troponin and its components. *J. Biochem. (Tokyo)*, **69**, 441–445.
30. Shitaka, Y., Kimura, C., Iio, T. & Miki, M. (2004). Kinetics of the structural transition of muscle thin filaments observed by fluorescence resonance energy transfer. *Biochemistry*, **46**, 10739–10747.
31. Miki, M., Hai, H., Saeki, K., Shitaka, Y., Sano, K.-I., Maéda, Y. & Wakabayashi, T. (2004). Fluorescence resonance energy transfer between points on actin and the C-terminal region of tropomyosin in

skeletal muscle thin filaments. *J. Biochem. (Tokyo)*, **136**, 39–47.
32. Monteiro, P. B., Lataro, R. C., Ferro, J. A. & Reinach, F. C. (1994). Functional alpha-tropomyosin produced in *Escherichia coli*. A dipeptide extension can substitute the amino-terminal acetyl group. *J. Biol. Chem.* **269**, 10461–10466.
33. Kunkel, T. A. (1985). Rapid and efficient site-specific mutagenesis without phenotypic selection. *Proc. Natl Acad. Sci. USA*, **82**, 488–492.
34. Kluwe, L., Maeda, K., Miegel, A., Fujita-Becker, S., Maéda, Y., Talbo, G. *et al.* (1995). Rabbit skeletal muscle α-tropomyosin expressed in baculovirus-infected insect cells possesses the authentic N-terminus structure and functions. *J. Muscle Res. Cell Motil.* **16**, 103–110.
35. Tao, T., Lamkin, M. & Lehrer, S. S. (1983). Excitation energy transfer studies of the proximity between tropomyosin and actin in reconstituted skeletal muscle thin filaments. *Biochemistry*, **22**, 3059–3066.
36. Hudson, E. N. & Weber, G. (1973). Synthesis and characterization of two fluorescent sulfhydryl reagents. *Biochemistry*, **12**, 4154–4161.
37. Tausky, H. H. & Shorr, E. (1953). A microcolorimetric method for the determination of inorganic phosphorus. *J. Biol. Chem.* **202**, 675–685.
38. Scott, T. G., Spencer, R. D., Leonard, N. G. & Weber, G. (1970). Emission properties of NADH. Studies of fluorescence lifetimes and quantum efficiencies of NADH, AcPyADH, and simplified synthetic models. *J. Am. Chem. Soc.* **92**, 687–695.
39. Miki, M., Hambly, B. D. & dos Remedios, C. G. (1986). Fluorescence energy transfer between nucleotide binding sites in an F-actin filament. *Biochim. Biophys. Acta*, **871**, 137–141.